Applied Catalysis B: Environmental 220 (2018) 635–644

Contents lists available at ScienceDirect

Applied Catalysis B: Environmental

journal homepage: www.elsevier.com/locate/apcatb

Catalytic oxidation of aqueous organic contaminants by persulfate activated with sulfur-doped hierarchically porous carbon derived from thiophene

Yaoping Guo[a,b], Zequan Zeng[a,*], Youcai Zhu[c], Zhanggen Huang[a,*], Yan Cui[a], Jieyang Yang[a]

[a] State Key Laboratory of Coal Conversion, Institute of Coal Chemistry, Chinese Academy of Sciences, Taiyuan 030001, PR China
[b] University of Chinese Academy of Sciences, Beijing 100049, PR China
[c] School of Environment and Chemical Engineering, Shanghai University, Shanghai 200444, PR China

ARTICLE INFO

Keywords:
Sulfur-doped
Hierarchically porous carbon
Persulfate
4-Chlorophenol
Aqueous organics

ABSTRACT

Sulfate radicals ($SO_4\cdot^-$) generated from persulfate (PS) activated by carbocatalysis is expected to provide an environmentally friendly and highly efficient catalytic oxidation process for aqueous organics degradation. Herein, a novel sulfur-doped hierarchically porous carbon with both structural and compositional modification was proposed for PS activation by using thiophene as sulfur/carbon precursor and KOH as activator. The effect of annealing temperature on its textural properties and surface chemistry was characterized by Elemental analysis, N_2 sorption isotherms, X-ray photoelectron spectroscopy, Fourier transform infrared spectra, Raman spectra and X-ray diffraction. The as-prepared sample treated at 800 °C (SDAC-800) demonstrated outstanding catalytic activity for activation of PS to degrade 4-chlorophenol (4CP). Studies on the role of sulfur in the catalytic activity enhancement were carried out by comparing with a sulfur-free activated carbon and a carbon model (reduced graphene oxide (rGO)). The effects of catalyst dosage, initial 4CP concentration, and reaction temperature on 4CP degradation were comprehensively investigated. In addition, contrast tests with other conventional PS activation methods, SDAC-800 reusability and its general applicability tests were also carried out. The mechanism of PS activation and 4CP oxidation was elucidated by using quenching tests with chloridion, L-histidine and ethanol as radical scavengers. It revealed that the conventional radical pathway was not a critical role in 4CP degradation. In contrast, the process was controlled by both particle-surface interaction and non-radical pathway, and the latter played a dominant role.

1. Introduction

With the rapid development of industry, industrial wastewater inevitably contains a large number of hazardous substances, such as particles, toxic refractory organics, and heavy metals [1], which has been far beyond the natural degradation ability by the ecosystem [2]. Owing to the challenges from environmental pollution, green technologies for environmental remediation have been extensively investigated [3]. In terms of organic contaminants in wastewater, advanced oxidation processes (AOPs) based on highly reactive radicals were widely acknowledged to be one of the most excellent and powerful technologies since they can provide an almost total degradation [4].

Recently, AOPs based on sulfate radical ($SO_4\cdot^-$) generated from persulfate (PS) or peroxymonosulfate (PMS) have attracted much attention for aqueous organics oxidation. $SO_4\cdot^-$ possesses a high oxidative potential (E_0 = +2.5 to +3.1 V vs. NHE), a longer lifetime ($t_{1/2}$ = 30–40 μs of $SO_4\cdot^-$ versus $t_{1/2}$ = < 1 μs of HO· [5]), and a wide operative pH range as well as avoiding the flocculation [6–8], which can be a promising alternative to the classic hydroxyl radical (HO·)-based Fenton reaction. Therefore, more studies were focused on the development of PS/PMS activation technologies for $SO_4\cdot^-$ generation. The conventional approaches such as thermal treatment and UV irradiation [9–11] have been found to be efficient for PS/PMS activation but they were at the expense of high energy inputs. Transition metals (Fe(II), Co(II), Ag(I), Fe^0) catalysis [12–15] was demonstrated the most simple and efficient method, attributing to the variable valency of transition metals. The empty orbitals of the outer shell could easily bond with PS/PMS molecules and then facilitate the electron transfer process involving reduced/oxidized metal ions [16,17]. In addition, it was reported that the peroxides could also be activated by metal oxides or metal oxides-based heterogeneous catalysts such as Fe_3O_4, α-MnO_2, Co_3O_4, and $LaCoO_3$ [18–23]. Nevertheless, the possible secondary pollution and toxic metal leaching would impede their practical applications.

Based on these considerations, more research groups have focused their attention on the preparation of carbonaceous materials for $SO_4\cdot^-$

* Corresponding authors.
E-mail addresses: zengzequan@sxicc.ac.cn (Z. Zeng), zghuang@sxicc.ac.cn (Z. Huang).

http://dx.doi.org/10.1016/j.apcatb.2017.08.073
Received 5 June 2017; Received in revised form 5 August 2017; Accepted 21 August 2017
Available online 25 August 2017
0926-3373/

generation due to their non-toxicity, excellent regulation performance, porous structure, and good thermal stability [8,24,25]. Studies on carbocatalysis demonstrated that carbon materials, such as activated carbon (AC), reduced graphene oxide (rGO), carbon nanotubes (CNTs), and nanodiamond (ND) can be also employed as activator for PS/PMS oxidation of organic contaminants [17,26–28]. While the catalytic oxidation process on carbocatalysis was much different from the metal-based catalysis. It was widely accepted that the generated reactive radicals contributed to the rapid degradation of organics. But in some carbocatalysis systems, it was proposed that the processes were dominated by the surface-bound radicals or the non-radical mechanism [16,17,29].

It was expected that structural modification and chemical compositional modification would bring about intrinsic changes to the catalytic activity of carbon materials. Therefore, the addition of activating reagent and the doping of heteroatom were widely investigated [6,30–35]. Sun et al. [1,6,32] demonstrated that GO, rGO and CNTs with nitrogen doping showed enhanced performance in PMS activation for organics oxidation. Also, sulfur could act as a promising co-dopant to further improve the performance of nitrogen doped graphene toward PMS activation [36]. Although these modified carbon materials show high performance to activate PMS or PS, the preparation of the samples is relatively complex, expensive and even involves harsh treatment. Therefore, simple, cheap and available synthesis would be more favorable. In addition, post-treatment of carbonaceous materials with heteroatom precursors fails to incorporate heteroatom into sp2 carbon networks [32]. Thus the surface functionalization may lead to the decrease of surface area, and the loss of heteroatom-based functional groups due to the weak anchoring between heteroatom groups and the basal surface of carbon [37]. In this regard, in-situ process could make sulfur groups homogeneously distributed throughout the matrix and permanently fused into the backbone of the carbon framework [37]. In the previous study, we first discovered that unitary sulfur doped porous carbon with 2-thiophenemethanol as S/C precursor and KOH as activator exhibited outstanding catalytic activity for PS oxidation of 4-chlorophenol (4CP) [38]. As 2-thiophenemethanol is very expensive (¥980/100 g), search for low-cost S/C precursors would be much economic and favorable for wastewater remediation. In addition, the mechanism of PS activation on this emerging carbocatalysis is still not fully understood.

Herein, we proposed an efficient and low-cost route towards sulfur-doped hierarchically porous carbon (SDAC). The carbons were constructed by using thiophene as precursor and KOH as activator under different annealing temperatures. The resultant samples were employed as catalysts for activation of PS to degrade aqueous organic contaminants. The effects of annealing temperature on their textural properties and surface chemistry were characterized in detail. The role of sulfur in catalytic activity enhancement was illustrated by comparing with a sulfur-free activated carbon and a carbon model (reduced graphene oxide (rGO)). Classic quenching tests were employed to uncover the mechanism of PS activation on SDAC. It is expected that the SDAC/PS system would be an environmentally friendly and efficient technology for wastewater remediation.

2. Experimental

2.1. Reagents

Thiophene (C_4H_4S, 97%), ferric trichloride ($FeCl_3$), and potassium persulfate ($K_2S_2O_8$) were purchased from Aladdin. Acetonitrile (C_2H_3N) was purchased from walk world chemical reagent co., Ltd. (Shanghai, China). 4-chlorophenol (C_6H_5ClO, ≥99.0%), 2,4-dichlorophenol ($C_6H_4Cl_2O$), 4-acetamidophenol ($C_8H_9NO_2$), sodium methylparaben ($C_8H_7NaO_3$) and salicylic acid ($C_7H_6O_3$) were obtained from Sigma-Aldrich. Other reagents used in this study were provided by Taiyuan Chemicals Co. (Taiyuan, China). All chemicals were of analytical grade or higher and used as received without further purification. Milli-Q water was employed throughout the experiments.

2.2. Preparation of sulfur-doped hierarchically porous carbon (SDACs)

In-situ S-doped activated carbons (SDACs) were synthesized by chemical activation of polythiophene (PTh) with KOH as activator under different annealing temperatures (Scheme S1). Firstly, polythiophene (PTh) was prepared using thiophene as starting material and $FeCl_3$ as initiator. Typically, 32 g of $FeCl_3$ was dissolved into 100 mL of CH_3CN, then 200 mL of CH_3CN dissolving 3.4 g of thiophene was slowly added with magnetically stirring. After stirring for 24 h at room temperature, the polymers were collected and washed with acetone and acetonitrile several times to remove the residue, then dried at 65 °C in vacuum for 24 h to obtain PTh.

Thereafter, SDACs were prepared by chemical activation of PTh with KOH as activator. In a typical synthesis, PTh and KOH with a weight ratio of 1:2 was dispersed into 50 mL of water, dried in an oven at 105 °C for 12 h, and finally subjected to annealing in a tubular furnace under nitrogen atmosphere (3 °C min^{-1}) at 600, 700, 800 °C for 1 h to obtain SDAC-600, -700, and -800, respectively. In the annealing process, the textural properties, sulfur doping levels and the loading of functional groups can be tuned by controlling the annealing temperature. After cooling to room temperature in nitrogen atmosphere, the activated samples were washed with 10 wt.% HCl solution twice and ultrapure water several times to remove any impurities, following by drying in an oven at 110 °C overnight. Finally, all the yielded sulfur-doped hierarchically porous carbons were stored in a desiccator prior to use. For a comparison, a sulfur-free porous carbon was prepared similarly but with annealing of polyphenylether (PPO) at 800 °C instead of PTh. The resultant sample was denoted as AC-800.

2.3. Cost analysis of the SDAC-800 sample

According to the price and the consumption of raw material in the catalyst preparation processes (Table S1), cost analysis of the SDAC-800 sample was conducted and compared with our previous prepared sulfur doped porous carbon (ACS) with 2-thiophenemethanol as S/C precursor [38]. Results show that compared with ACS, the cost of the SDAC-800 sample was greatly reduced (Supporting information).

2.4. Characterization of materials

Elemental analysis (EA) was performed by using a Vario EL CUBE elemental analyzer with the oxygen content calculated by mass difference. Thermogravimetric analysis (TGA) was conducted in a Netzsch thermal analyzer in an air atmosphere with a heating rate of 5 °C min^{-1} from 25 °C to 800 °C. The textural properties of the materials were determined by nitrogen sorption isotherms at 77 K using a TriStar II 3020. All samples were degassed at 80 °C for 8 h under vacuum before measurement. The specific surface area was calculated by the Brunauer-Emmett-Teller (BET) equation. The total pore volume was calculated from the volume adsorbed at a relative pressure of 0.99. The Dubinin-Astakhov equation adapted for micro-pore carbon was applied to detect the micropore surface area and micropore volume of the as-prepared samples, and Original Density Functional Theory (ODFT) were applied to determine the pore size distribution (PSD). Scanning electron microscope (SEM, JSM-7001F, JEOL, Japan) was used to observe the morphologies of the samples. X-ray photoelectron spectroscopy (XPS) was performed on a specs spectrometer (AXIS ULTRA DLD) using Al Ka X-ray source (1486.6 eV). Fourier transform infrared spectra (FTIR) were recorded on a Bruker Tensor 27 FTIR spectrometer fitted with a transmission attachment. Raman spectra were acquired on a Horiba (LabRAM HR800) dispersive Raman spectrometer using argon ion laser source with λ at 514 nm. X-ray diffraction (XRD) patterns were obtained on a Bruker D8-Advanced diffractometer system using Cu-Kα

radiation (λ = 1.5418 Å). The pHpzc (point of zero charge) of the samples were evaluated by dispersing 250 mg of carbon samples into 4 mL of CO_2-free water at 25 °C [39].

2.5. Catalytic oxidation of aqueous organic contaminants

The batch catalytic oxidation of aqueous contaminants was carried out to evaluate the catalytic performance of SDACs on PS activation. The experiment was conducted in a 250 mL conical flask containing 200 mL of contaminant solution (80 mg L^{-1}), 0.1 g L^{-1} of catalyst, and 15 mM of $K_2S_2O_8$. The flask was shaken in a constant temperature shaker (TENSUC Instrument, TS-200B, China) with the temperature set at 25 °C. At given time intervals, 1 mL of reaction solution was withdrawn and filtered by 0.22 μm millpore film into a HPLC vial for analysis. Blank tests with addition of PS only or catalyst only were also carried out. All the experiments were performed in duplicates, and the results showed that the relative errors were less than ± 5%.

The concentrations of residual contaminants and intermediates were determined by using a high performance liquid chromatography (HPLC, UltiMate3000, Thermo Fisher, USA) equipped with a SunFire™ C_{18} column (4.6 × 150 mm, 5.0 μm) and a photodiode array detector (PDA). The mobile phase was a binary mixture of 70% methanol and 30% water at a flow rate of 1 mL min^{-1}. Chemical oxygen demand (COD) was determined by a COD analyzer (5B-3A, Lian-hua Tech. Co., Ltd., Lanzhou, China) according to the Chinese national standard method (HJ/T 399–2007). PS concentrations were measured by UV spectrophotometric method [40].

3. Results and discussion

3.1. Materials characterization

Table 1 presents the elemental compositions of the SDACs. As the rise of annealing temperature, the contents of oxygen and sulfur were significantly reduced due to the removal of excessive groups with low stability. Remarkably, the sulfur doping level dropped greatly from 12.96 wt.% to 4.89 wt.% as the annealing temperature increased from 600 to 800 °C. Nevertheless, compared with previous research concerning S-doping carbons [38,41–44] as concluded in Table S2, the sample treated at 800 °C still showed a high quantity of S-doping level. It is suggested that thiophene could act as an excellent and efficient sulfur precursor for in situ S-doped porous carbons.

The thermogravimetric analysis (TGA) showed that there almost no residue was remained after the combustion of carbon samples. It indicates that the iron compounds derived from $FeCl_3$ has been fully removed, demonstrating the metal-free of SDACs (Fig. S1).

It is well established that the textural properties of porous carbons are significantly influenced by the annealing temperature during carbonization. As presented in Table 1, both micropore surface area (S_{micro}) and micropore volumes (V_{micro}) increased steadily with increasing annealing temperature. This can be attributed to a progressing carbonization process accompanied by release of volatile species at an elevated temperature [30], giving rise to the development of micropores. Moreover, an improving specific surface area (S_{BET}) and total pore volume (V_p) were also observed on SDACs prepared at elevated temperature, concurrently, their corresponding average pore size increased from 1.99 to 2.06 and then to 2.14 nm. It was suggested that high calcination temperature was more conductive to the development of porous structures, but excessively high temperature would give rise to the collapse of the carbon skeleton structure and then enlarge the pore size of the material, hence leading to a higher V_p [6]. As confirmed by the pore size distributions of SDACs (Fig. 1b), the porosity of the SDACs were mainly made up of micropores (< 1.2 nm) and a certain enlargement of the pore size to mesopore range (2–4 nm) was observed with an increase of annealing temperature. According to N_2 sorption isotherms as shown in Fig. 1a, all the SDAC samples presented type I isotherms with narrow hysteresis loops and large adsorption capacities at low relative pressure, followed by a moderate increase at relatively intermediate pressures, indicating the generation of hierarchically porous of SDACs [36]. Compared with SDACs, AC-800 possessed the largest S_{BET} and V_p with a typical type I isotherm.

XPS spectroscopic technique was conducted to detect the surface atomic concentration (at.%) and the surface chemistry of the carbon samples. As shown in Fig. 2a, three characteristic peaks attributed to sulfur, carbon, and oxygen were observed on the full XPS spectra of SDACs with binding energies at 167.5, 284.5, and 532.5 eV, respectively. It can be found that thermal treatment at higher temperature would result in significant heteroatoms loss. Remarkably, the atomic ratios of sulfur decreased from 3.60 at.% to 1.79 at.% and then to 1.37 at.% for SDAC-600, −700, −800, respectively, which was consisted roughly with the elemental analysis results (Table 1).

Fig. 2b–d reveals that the C1 s XPS spectra can be decomposed into five components. The main peak at 284.5 eV is assigned to carbon atoms with sp^2 hybridization. The peak at 285.8 eV could be attributed to sp^2 carbon bonded with heteroatoms such as C—O and/or C—S [33]. The band on the high binding energy side can be deconvolved into a peak centered at 287.2 eV corresponds to C═O species (carbonyl or quinine), and a peak centered at 289.2 eV corresponds to O═C—O (carboxyl or ester). The signal at 291.2 eV is possibly assigned to the π-π* transition due to conjugation [45]. Their corresponding concentrations were summarized in Table S3.

High resolution S 2p XPS spectra were obtained to investigate the types of S-containing species (Fig. 2e). It is noted that all the S 2p peaks of SDACs can be deconvolved into four components. The two peaks at 164.0 eV and 165.2 eV are attributed to the S $2p_{3/2}$ and S $2p_{1/2}$ of thiophene sulfur (—C—S—C—), and the other two peaks with higher binding energies of 168.8 eV and 169.9 eV are assigned to oxidized S (—C—SO_x—C—, x = 2, 3, 4) [33,42,46]. We found that the concentrations of —C—S—C— were 1.63 at.%, 0.90% at.%, and 0.89 at.% in SDAC-600, -700 and -800, respectively, but the percentage of —C—S—C— in overall S dopants increased with a level of 45.36%, 50.23%, and 64.74% accordingly. It is well known that a higher temperature could break up the C—S bond and cause sulfur depletion, whereas elevated temperature could also afford more instinct incorporation of S into the carbon framework. Yang and his co-workers [43] reported that the oxidized sulfur species can be transformed into sulphide groups at higher annealing temperature due to their lower stability. This may be favorable because S—C bonds are presumed to be important active sites

Table 1
Elemental compositions and textural properties of the carbon samples.

Sample	Elemental composition (wt.%)					Textural properties			
	C	H	O	S	N	S_{BET} ($m^2 g^{-1}$)	S_{micro} ($m^2 g^{-1}$)	V_p ($cm^3 g^{-1}$)	V_{micro} ($cm^3 g^{-1}$)
SDAC-600	65.31	1.55	19.88	12.96	0.30	1302	1114	0.65	0.43
SDAC-700	80.07	0.81	9.91	8.69	0.52	1645	1145	0.85	0.47
SDAC-800	90.05	0.53	4.12	4.89	0.41	1740	1212	0.93	0.50
AC-800	88.82	1.44	9.37	/	0.37	2182	1682	1.06	0.67

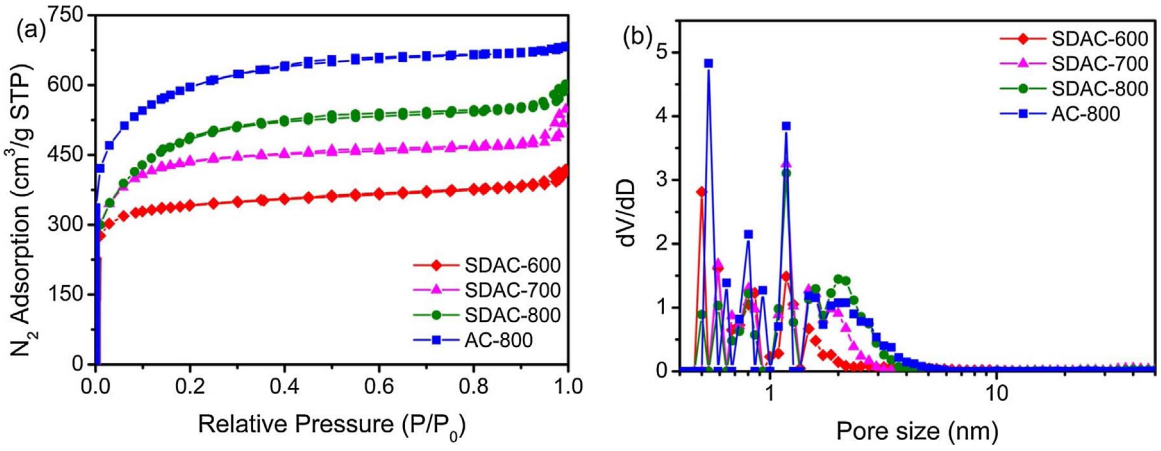

Fig. 1. (a) N_2 sorption isotherms, and (b) pore size distributions of the carbon samples.

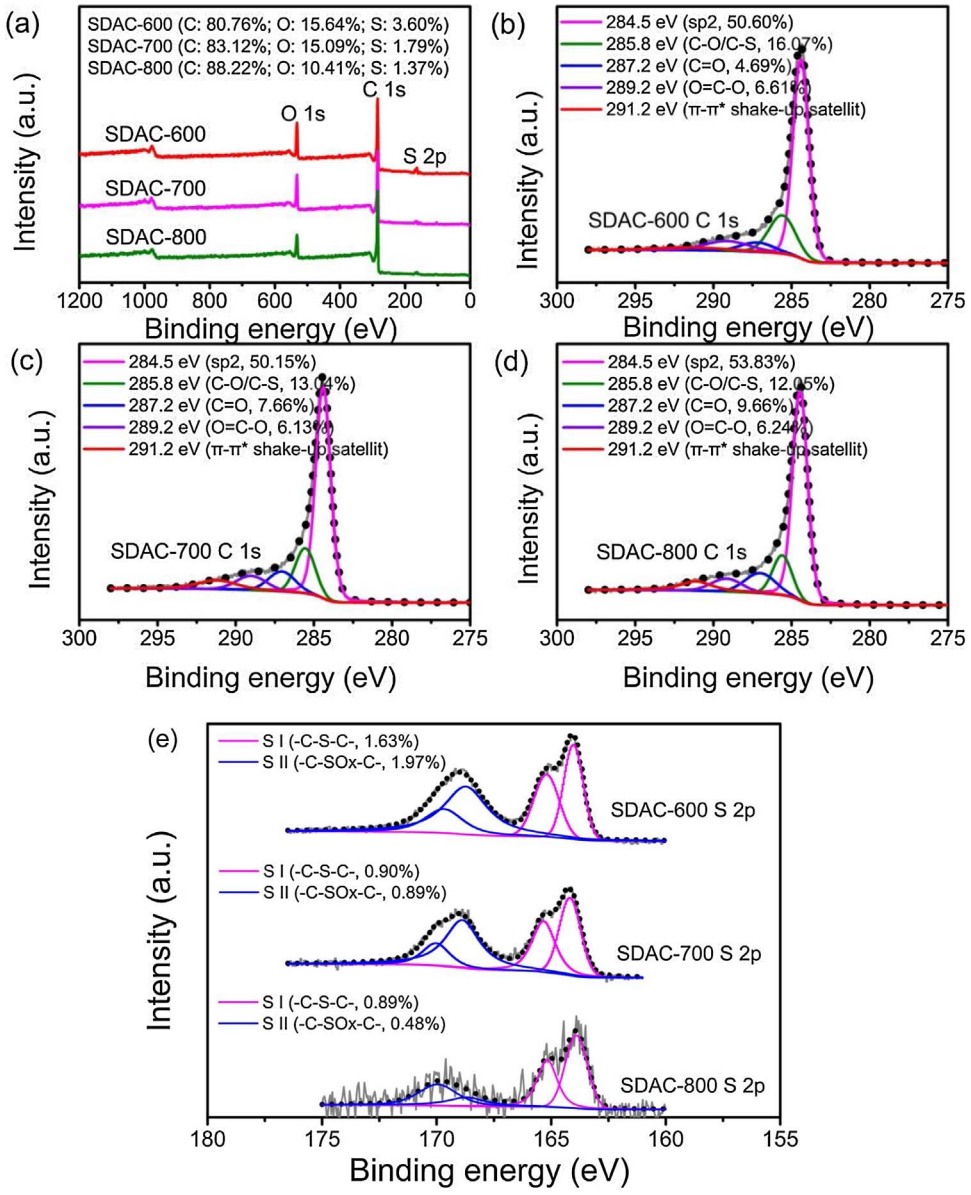

Fig. 2. (a) XPS survey of SDAC-600, -700, -800, (b)-(d) C 1s scan, and (e) S 2p scan of SDAC-600, -700, -800, respectively.

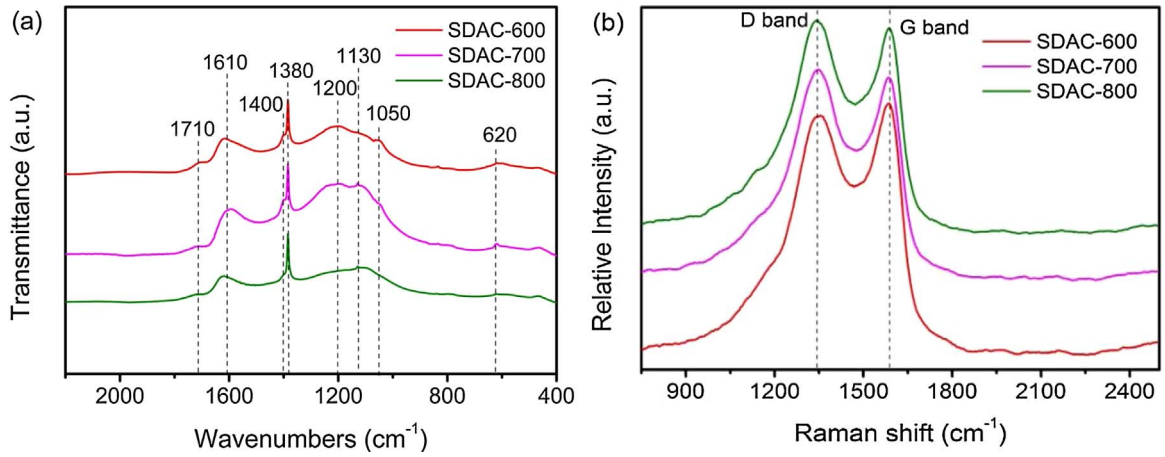

Fig. 3. (a) FTIR spectra, and (b) Raman spectra of SDAC-600, -700, -800, respectively.

for oxygen-reduction reaction (ORR) catalytic activity enhancement of materials [43].

FTIR spectra were recorded to further determine the nature of the chemical bonding between carbon and heteroatoms. As can be seen from Fig. 3a, the FTIR spectra show the C═C stretching vibrations in aromatic rings at 1610 cm^{-1} and 1380 cm^{-1}, respectively. The band located around 1710 cm^{-1} can be assigned to the stretching vibration of C═O in aldehydes or ketones [45]. The symmetric stretching vibration of O═C−O at 1400 cm^{-1} is also observed, and the band at 1050 cm^{-1} shows the presence of C−O−C in aromatic ether. The two peaks at 1130 cm^{-1} and 1200 cm^{-1} can be assigned to O═S═O stretching vibration caused by some oxidized sulfur, and the low energy absorption band at 620 cm^{-1} is characteristic of C−S stretching vibration in thiophene sulfur [47]. It is worth noting that thermal treatment at high temperature leads to the vanishing of the bands characteristic of oxidized sulfur at 1200 cm^{-1} as well as aromatic ether groups (1050 cm^{-1}), and weakens the intensity of the O═C−O groups. This indicates that a better reducibility is achieved on SDAC-800.

Raman spectroscopy is a powerful tool to reflect the defect and disorder level of carbonaceous materials [6,33]. The degree of disorder in the structure can be evaluated by calculation the I_D/I_G ratio (the intensity ratio of D band versus G band), where D band is related to the defects in sp^2 lattice and G band is related to graphitic structure. A high I_D/I_G ratio means a high number of defect sites. As shown in Fig. 3b, the strong D band at 1349 cm^{-1} and the strong G band at 1582 cm^{-1} [33] were observed on all SDACs, and the I_D/I_G values were determined to be 0.96 for SDAC-600, 1.02 for SDAC-700, and 1.08 for SDAC-800. It is concluded that SDACs can be tailored with more defect sites at higher thermal annealing, which could also be confirmed by the results of SEM, and XRD (Fig. S2 and S3).

3.2. Catalytic activity of materials

3.2.1. Catalytic oxidation of 4CP

The adsorptive and catalytic performances of SDAC samples were first evaluated by 4CP removal as shown in Fig. 4a. It can be seen that 4CP adsorption on the SDAC samples was a fast process, and the absorption equilibrium could be reached during 10 min. In the absorption tests, about 30.7%, 37.5% and 41.8% of 4CP was removed on SDAC-600, -700, and -800, respectively. Accordingly, their adsorption capacities on unit S_{BET} (q_e/S_{BET}) were estimated as 0.187, 0.183, and 0.192 mg m^{-2}. Therefore, one can conclude that the adsorption abilities of the SDAC samples were basically in accordance with their S_{BET}.

With the addition of PS only, no 4CP degradation was observed. While the degradation process can be significantly enhanced by introduction of SDACs into the above systems. By deducting their respective adsorption contributions, about 17.3%, 43.3% and 58.2% of extra 4CP was removed on SDAC-600, -700 and -800 during a reaction time of 90 min, respectively.

Fig. 4b shows that the activation of PS on SDACs followed a first-order kinetics behavior, and the apparent decomposition rate constant of PS on SDAC-800 was 2.76 × 10^{-3} min^{-1}, being about 3.6 times that on SDAC-700, and 12.27 times that on SDAC-600. The corresponding COD removal efficiencies of SDAC/PS were displayed in Fig. 4b (inset). As observed, SDAC-600, -700 and -800 with PS provided about 32%, 53%, and 68% COD removal, respectively. These results strongly

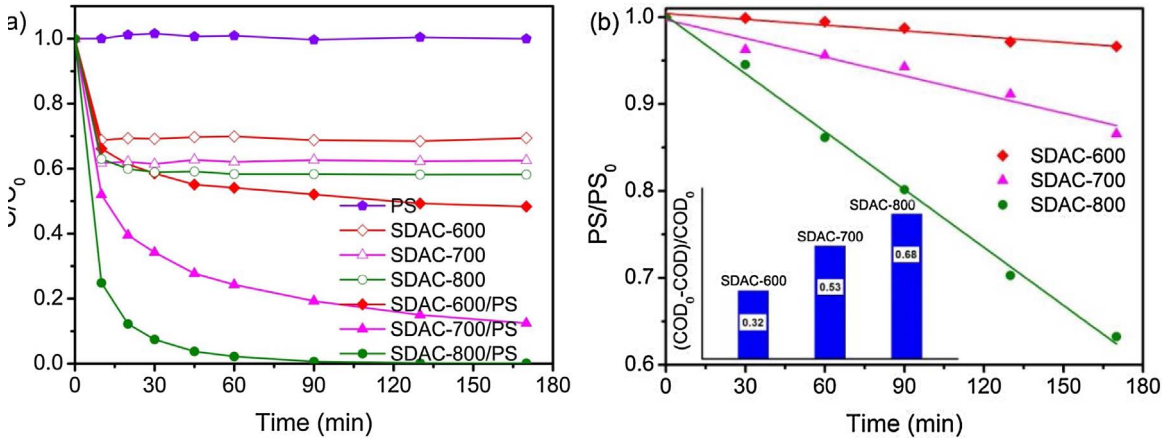

Fig. 4. (a) The removal of 4CP under various reaction systems, and (b) the decomposition of PS and COD removal (inset) on SDAC-600, -700, -800, respectively. Reaction conditions: $[4CP]_0$ = 80 mg L^{-1}, catalyst = 0.1 g L^{-1}, [PS] = 15 mM, and temperature = 25 °C.

indicated that the catalytic activities of the SDAC samples toward PS activation were significantly influenced by their annealing temperature. In the temperature range of 600–800 °C, the sample treated at higher temperature exhibited an increased activation potential for PS oxidation of 4CP.

On the basis of the adsorption and oxidation tests, it is concluded that surface chemistry properties of SDACs played more important role than S_{BET} in the catalytic activity enhancement of carbon samples. It was suggested that the sp2 carbon with abundant free-flowing electrons, the electron rich oxygen-containing functionalities, and the defect sites with delocalized π electrons were possibly the active sites for PS/PMS activation [48,49]. Also the C–S bands were presumed to play a vital role in the ORR catalytic activity [43]. Associated with the XPS survey of SDAC samples (Table S3), it is noted that a better catalytic performance was obtained with a higher concentration of sp2 hybridized structure, O═C groups, and defect sites, but no positive correlation was observed between total sulfur content and catalytic 4CP oxidation. Whereas it is worth noting that the percentages of the oxidized sulfur groups with acid character were significantly reduced with an increase of annealing temperature. As revealed by the pH_{PZC} values (Table S3), SDAC-600 and SDAC-700 possessed evident strong acidic characters with low pH_{PZC} values of 1.2 and 1.6, respectively. In contrast, SDAC-800, due to the removal of large amounts of sulphone groups, was characterized as a weak acidic material with pH_{PZC} of 4.2. It is well established that activated carbons with a basic character would be favorable to the catalytic oxidation, since most of the acidic active sites had an electron withdrawing capacity [34]. Therefore, we speculate that the significant removal of sulphone groups at high temperature also played a key role in catalytic activity enhancement of SDAC-800, since the increased reducibility of the carbon surface was conducive to the electron-transfer from SDAC-800 to PS.

The role of the sulfur dopant in the catalytic 4CP oxidation was studied by the comparison tests of sulfur-free activated carbon (AC-800) as shown in Fig. 5. The experiment results showed that AC-800 sample possessed a higher adsorption ability (50.9%) due to its huger S_{BET}, but showed an inferior catalytic performance with 86.5% of 4CP removal in 90 min when compared with SDAC-800 (100%). The XPS spectra and Raman spectrum of AC-800 were recorded (Fig. S4 and Fig. S5). It revealed that similar amounts of C═O, lower concentrations of sp2 hybridized structure, and less defect sites were detected on the AC-800 surface (Table S3). Therefore, we speculate that: (i) the sp2 structure and defect sites may play important roles as the active sites in PS activation; (ii) sulfur doping may strongly enhance the catalytic activity of carbon towards PS activation.

It is widely accepted that reduced graphene oxide (rGO) is a common carbon material with sp2 structure, functional groups and defect sites [50]. Thus, to assess the contribution of these possible active sites for PS activation, rGO was applied as the carbon model for comparison (Fig. 5 (inset)). As seen, by deducting its adsorption contribution, about 35.9% of extra 4CP was removed on rGO in 90 min, which was comparable to that of AC-800 (35.6%) and much lower than that of SDAC-800 (58.2%). To conclude, the sulfur doping significantly improved the PS-activating ability of carbon samples. Kicin´ski et al. [37] reported that element S with a large atom radius could generate structural defects in the carbon crystal lattice, which in turn results in more edge-active sites, leading to the catalytic performance enhancement. It was well established that the thiophenic sulfur species inserted into the sp2-hybridized carbon lattice could bring high spin density to the neighboring carbon atoms and facilitate charge localization [37], hereby altering the electron configuration of the sp2 carbon and creating more active sites for the catalytic activity enhancement. Moreover, the sulfur presented in −C−S−C− acting as bridges between adjacent aromatic rings (sulphide bridges) is rich in electrons. It could transfer electrons to the electrophilic oxygen of persulfates, giving rise to the activation of PS. As the effects of the sulfur dopant on the electron states of carbon atoms cannot be uncovered here, density functional theory (DFT) calculations are still need to be done to explore the role of sulfur in PS activation process in future studies.

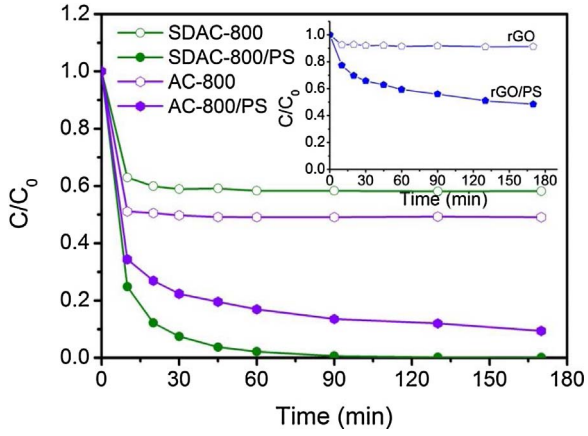

Fig. 5. The removal of 4CP on SDAC-800, AC-800, and rGO (inset), respectively. Reaction conditions: $[4CP]_0$ = 80 mg L^{-1}, catalyst = 0.1 g L^{-1}, [PS] = 15 mM, and temperature = 25 °C.

3.2.2. Effects of several parameters on the catalytic activity of SDAC-800

To gain further insight into the effects of reaction parameters on 4CP degradation, SDAC-800 was chosen for the tests in the following sections because of its excellent catalytic performance. Fig. S6 depicts the effect of SDAC-800 dosage on 4CP removal. It revealed that the oxidation efficiency significantly increased with an increase of SDAC-800 dosage. Around 78% 4CP removal was achieved in 170 min with a dosage of 0.05 g L^{-1}, whereas 100% of 4CP can be removed in 90 min and 30 min at 0.1 g L^{-1} and 0.15 g L^{-1}, respectively. It is because that a higher catalyst dosage would provide huger specific surface area and more active sites for the generation of sulfate radical, thereby improving the degradation process. Fig. S7 shows the influence of initial 4CP concentration on its degradation rate in the range of 60–100 mg L^{-1}. Although the degradation rate at higher initial concentration seemed to be slower due to the excessive occupation of the active sites of the catalyst and the lack of PS, a complete 4CP removal could still be achieved in 170 min at an initial 4CP concentration of 100 mg L^{-1}, suggesting the high catalytic activity of the SDAC-800 sample.

Fig. 6a illustrates the effect of reaction temperature on 4CP removal over SDAC-800. It can be seen that the degradation rate increased with the increase of reaction temperature. Specifically, at 25 °C, 100% 4CP removal was achieved in 90 min, which can be shorten to 45 min under the condition of 55 °C. The kinetics data showed that the degradation of 4CP obeyed pseudo-first-order kinetics and the apparent reaction rate constant was evaluated to be 0.0975 min^{-1} at 55 °C, being about 1.64 times that (0.0596 min^{-1}) at 25 °C. Based on the Arrhenius equation, the activation energy of 4CP removal in SDAC-800/PS system was evaluated to be 13.53 kJ mol^{-1}, which was much lower than that on the AC-800 (29.75 kJ mol^{-1}), and rGO (33.40 kJ mol^{-1}) (Fig. S8).

Further studies were carried out to detect the reusability of the SDAC-800 sample. After each reaction cycle, the used catalyst was collected and washed with ultrapure water several times, followed by drying in an oven at 110 °C overnight for reuse tests. As shown in Fig. 6b, 56% and 15% of 4CP removal were achieved in the second and third runs within 210 min, respectively, indicating that the catalyst was deactivated seriously after several times employment. To explore the deactivation reason, the catalyst after 3rd run was characterized. N_2 sorption isotherms shows that its S_{BET} and pore volume significantly decreased due to the coverage of pore structures and active sites by the adsorbed 4CP molecules and its intermediates (Table S4), confirmed from pore size distribution (Fig. S9), thereby resulting in an inferior adsorption capacity and oxidation efficiency on 4CP. Also, both XPS

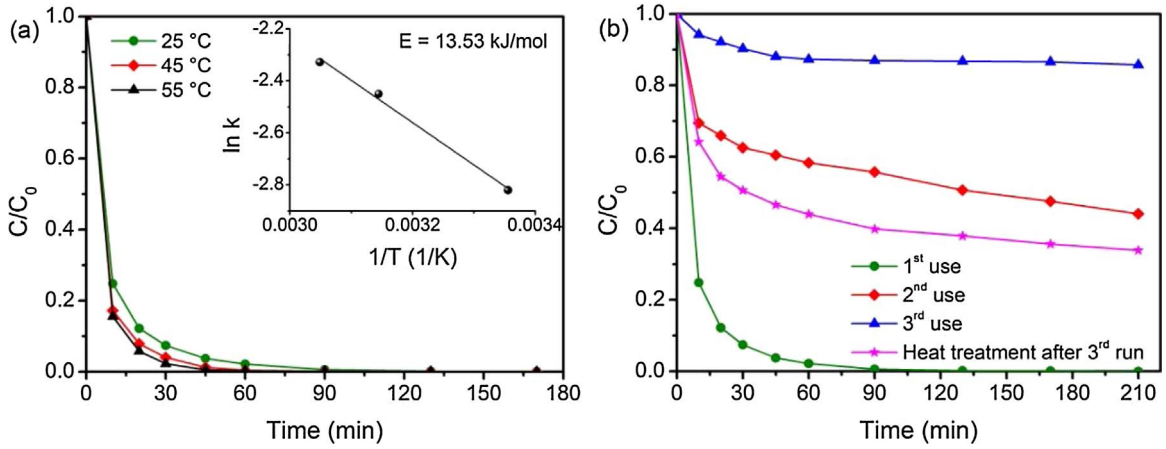

Fig. 6. (a) Effect of reaction temperature on 4CP removal in SDAC-800/PS system and estimation of activation energy (inset), and (b) performance of SDAC-800 upon successive uses. Reaction conditions: $[4CP]_0$ = 80 mg L^{-1}, catalyst = 0.1 g L^{-1}, [PS] = 15 mM.

(Fig. S10) and FTIR (Fig. S11) results show that the catalyst surface was partially oxidized under the highly oxidative environment. Remarkably, the percentage of −C−SO_x−C− in overall S dopants increased from 35.26% to 59.08% after three runs (Fig. S10(b)), indicating the attachment of sulfur oxides on the SDAC-800 surface derived from the attached sulfate radicals or the reactive PS complexes. The change of S-containing groups on SDAC-800 led to a less reductive surface and was not favorable for the electron transport from carbon to persulfate, hereby decreasing the PS activation and 4CP degradation. Thus, to recover the pore structure and the surface chemistry of the passivated SDAC-800 after 3 rdrun, a thermal treatment (annealing at 450 °C in N_2 for 1 h) was applied. Results show that its catalytic activity was only partially recovered with around 68.0% 4CP removal in 210 min. Nitrogen sorption isotherms shows that although the S_{BET} and pore volume greatly increased to 1216 m^2 g^{-1} and 0.71 m^3 g^{-1}, respectively, it was still not comparable to the fresh catalyst (1740 m^2 g^{-1} and 0.93 m^3 g^{-1}, respectively) (Table S4). In addition, both XPS and FTIR show that although a better reductive degree of the catalyst was obtained owing to the removal of adsorbed organics and/or the attached sulfur oxides, the content of the −C−SOx−C− group was still higher than that of the fresh catalyst, which has been demonstrated unfavorable for the electronic transport process. Thus, we suppose that the still inferior catalytic activity of the catalyst, even after a heat treatment, may be originated from the un-fully restored pore structure and surface chemistry. In this regard, further efforts should be made to develop efficient regeneration methods for the carbon material for future applications. The possible intermediate products were detected by HPLC, and the results were displayed in Fig. S12.

3.3. The general applicability of SDAC-800

For practical application, a superb catalytic performance and a good general applicability are critical for the catalyst. To gain further insight into the reactivity of SDAC-800 for organics oxidation, a brief comparison of catalytic degradation of 4CP by PS activated with different activation technologies was carried out as shown in Fig. 7a. It can be seen that the commercial Co_3O_4 and Fe_3O_4 metal oxides were not enable to activate PS. The carbon-based catalysts including reduced graphene oxide (rGO) and multi-walled carbon nanotubes (MWCNTs) with PS exhibited moderate oxidation abilities with about 51.6%, and 27.6% 4CP removal in 170 min, respectively. Thermal treatment at 55 °C provided 44.3% 4CP degradation during the same reaction time. In addition, we also investigated the degradation of 4CP in the classical zero-valent iron (ZVI)/PS system, and found that the system with 89.8% of 4CP removal was less efficient than SDAC-800/PS (100%). Accordingly, a comparison to conventional PS activation technologies allows us to conclude that SDAC-800 could act as a superb and effective persulfate activator for organics oxidation without secondary pollution.

In recent years, the removal of emerging contaminants has received increasing attention in environmental remediation, since their widespread use has brought some new environmental issues [5]. Therefore, several typical emerging contaminants, including 2,4-dichlorophenol (endocrine disruptor), 4-acetamidophenol (pharmaceutical), sodium methylparaben (preservative) and salicylic acid (personal care product), were applied to be degraded with PS activated by SDAC-800. As depicted in Fig. 7b, PS only presented negligible removal of these organics. When SDAC-800 was introduced into the above solution, the degradation efficiency of sodium methylparaben and salicylic acid could reach 88.7%, and 90.3% in 210 min, respectively. Remarkably, the fully degradation of 4-acetamidophenol and 2,4-dichlorophenol could be obtained in 20 min and 60 min, respectively. It indicates that all of the aforementioned emerging contaminants could be significantly degraded in SDAC-800/PS, even though they presented different degradation rates attributed to their diverse molecular structures and physicochemical properties [2]. It is demonstrated that SDAC-800 exhibits excellent generalization for the degradation of different emerging contaminants.

3.4. Quenching experiments and PS activation mechanism on SDAC-800

It has been well established that, in most AOPs, oxidants could be activated to form reactive radicals through conventional radical pathway, and the generated radicals played a dominant role for the destruction of organic contaminants [51,52]. Therefore, the degradation of target organics would be dramatically inhibited by the addition of radical scavenger into the reaction systems. More recently, Sun et al. [53,54] proposed a non-radical mechanism of PS/PMS activation by nitrogen doping carbon materials for organics oxidation. It was suggested that PS was first adsorbed on the surface of the carbon to form reactive complexes, and followed by rapid reaction with the adsorbed organics, where the degradation efficiency would not be fully inhibited even with a high concentration of radical scavenger. Lee et al. [28] also found the similar phenomenon in carbon nanotubes. In addition, it was reported that the radical generation process could also occurs at the solid-particle surface, namely, surface-bounded radicals [16,29].

Therefore, during the investigation of PS activation mechanism on SDAC-800, the role of free radicals in 4CP degradation process was first tested by using a quenching experiment. In these systems, a popular radical scavenger, chloride ion (Cl^-, with addition of NaCl) was used, since it can rapid interaction with $SO_4^{\cdot -}$ ($k_{SO4-\cdot}$ = 3.0 × 10^8 M^{-1} s^{-1}) and a small part of HO· produced in aqueous solution to form Cl, and then with another chloride in water to form

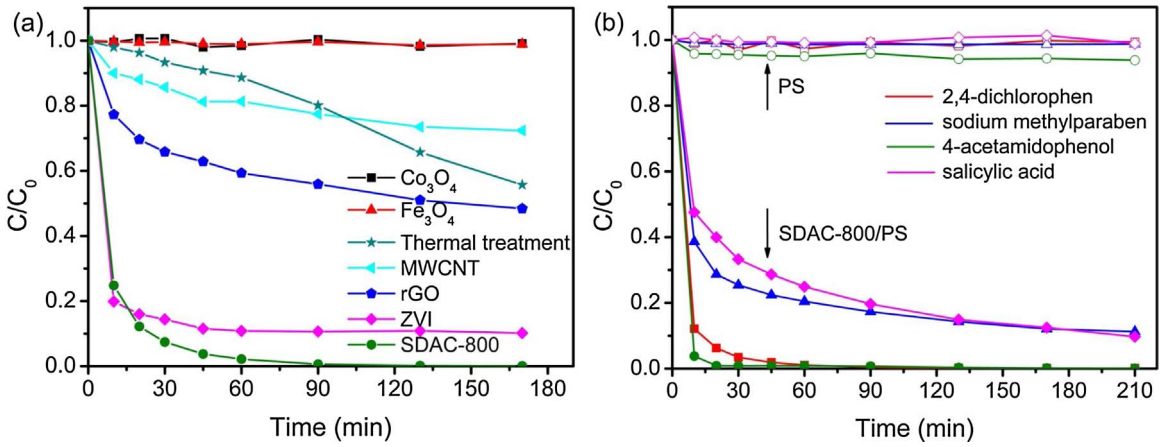

Fig. 7. (a) 4CP removal under various PS activation methods, and (b) the degradation of various emerging contaminants with SDAC-800/PS. Reaction conditions: $[contaminants]_0$: = 80 mg L^{-1}, except for salicylic acid (40 mg L^{-1}), catalyst = 0.1 g L^{-1}, [PS] = 15 mM, and temperature = 25 °C.

$Cl_2\cdot^-$ (Eqs. (1)–(5)) [29]. The chlorine radicals with a redox potential of 2.1 V were less reactive than $SO_4\cdot^-$ and HO· [16]. Therefore, if large amount of free radicals were generated in the two carbon/PS systems, the degradation rate of 4CP would slow down with the addition of Cl^-. However, no inhibitory effects were observed in both the SDAC-800/PS and AC-800/PS systems (Fig. S13). Then L-histidine was employed as singlet-oxygen ($^1O_2$) scavenger [17]. Results show that both adsorption and oxidation efficiency on 4CP were reduced with the introduction of excess amount of L-histidine (30, 60, 100 mM) (Fig. S14). However, by deducting adsorption efficiency, a minor inhibitory effect was observed on their corresponding oxidation efficiency, suggesting that almost no $^1O_2$ was generated in the SDAC-800/PS system, and the decreased adsorption and oxidation efficiency may be caused by the competitive adsorption between L-histidine and 4CP. From the obtained results, we can conclude that (i) the conventional radical mechanism was not the critical role in PS activation; (ii) the activation of PS was likely dominated by the non-radical pathway or the particle-surface interaction.

$$SO_4^{\circ-} + Cl^- \rightarrow SO_4^{2-} + Cl^{\circ} \quad (1)$$

$$Cl^{\circ} + Cl^- \rightarrow Cl_2^{\circ-} \quad (2)$$

$$HO^{\circ} + Cl^- \rightarrow ClOH^{\circ-} \quad (3)$$

$$ClOH^{\circ-} + H^+ \rightarrow Cl^{\circ} + H_2 \quad (4)$$

$$ClOH^{\circ-} + Cl^- \rightarrow Cl_2^{\circ-} + OH^- \quad (5)$$

To further disclose the activation mechanism in these systems, another radical quenching experiment was carried out. Ethanol, containing α–hydrogen, was employed as the probe compound for capture the total radicals generated in the PS activation process, owning to its high reactivity with both HO· and $SO_4\cdot^-$ ($k_{SO4\cdot-}$ = (1.6–7.8) × 10^7 M^{-1} s^{-1}, $k_{HO\cdot}$ = (1.2–2.8) × 10^9 M^{-1} s^{-1}) [53]. Results show that the 4CP degradation gradually decreased with the addition of excess amount of ethanol (Fig. 8). Especially, around 68% 4CP removal was achieved at an ethanol/PS molar ratio of 1000:1 within 210 min in the SDAC-800/PS system (Fig. 8a). However, it is worth noting that its corresponding adsorption capacity was also deceased with addition of the same amount of ethanol but without the presence of PS, attributing to the high solubility of 4CP in ethanol. By deducting its adsorption contribution, about 45.5% of extra 4CP was removed, which was slight lower than that of control test (58.2%). The degradation of 4CP on AC-800 also followed this pattern (Fig. 8b). It is suggested that both particle-surface interaction and non-radical pathway existed in the two carbon/PS systems, and the latter played a dominant role.

Accordingly, associated with the characterization results and the afore radical quenching experiments, the possible mechanism for PS activation on SDAC-800 was proposed as shown in Scheme 1. In the surface-bound radical oxidation process, the sp2 carbon structure with abundant free-flowing electrons, the electron-rich —C—S—C— groups (sulphide bridges) as well as carbonyl groups, and the defect sites with delocalized π electrons functioned as electron donors would transfer electrons to the electrophilic oxygen of persulfates, giving rise to the O—O bonding homolytic cleavage into surface-bounded sulfate radicals ($SO_4\cdot^-_{ads}$, an electron acceptor) (Eq. (6)). Then a part of $SO_4\cdot^-_{ads}$ react with H_2O (an electron donor) to produce $HO\cdot_{ads}$ (an electron acceptor) (Eq. (7)). On the contrary, $HO\cdot_{ads}$ could also be depleted through Eq. (8) to generate $SO_4\cdot^-_{ads}$. Then the adsorbed 4CP molecules as well as its intermediates as electron donors would be consequently oxidized into CO_2, H_2O, and Cl^- by the formed reactive radicals ($SO_4\cdot^-_{ads}$ and $HO\cdot_{ads}$) (Eq. (9)). Meanwhile, the radicals can be also consumed by some competitive reactions (Eqs. (10)–(13)), which bring about negative effect on the degradation process. In the non-radical process, the generated defects played an important role in activation of the sp2-hybridized carbon lattice. Then the activated sp2-hybridized carbon lattice would facilitate the electron transfer from SDAC-800 surface to PS for reactive complexes generation (electron acceptors), and followed by rapid reaction with the adsorbed 4CP molecules (electron donors) through charge transport. In addition, the thiophenic sulfur species inserted into the sp2-hybridized carbon lattice would bring high spin density to the neighboring carbon atoms and hence altering the electron configuration of the sp2 carbon and creating positively charged density on the adjacent C atoms, thereby contributing to the activation of sp2-hybridized carbon lattice. The inferior catalytic activity of AC-800 may be attributed to the lower concentration of active sites as discussed in Section 3.2.1 and the less amount of activated sp2-hybridized carbon lattice. Therefore, it can be concluded that sulfur doping not only enhances the surface-bound radical oxidation process but also enhances the non-radical pathway for PS activation, but the latter plays the dominant role in the 4CP degradation process.

$$S_2O_8^{2-} + e^- \rightarrow SO_4^{2-} + SO_4^{\circ-} \quad (6)$$

$$SO_4^{\circ-} + H_2O \rightarrow SO_4^{2-} + HO^{\circ} \quad (7)$$

$$HO^{\circ} + SO_4^{2-} \rightarrow SO_4^{\circ-} + OH^- \quad (8)$$

$$SO_4^{\circ-}/HO^{\circ} + 4CP \rightarrow \text{intermediates} \rightarrow CO_2 + H_2O + Cl^- \quad (9)$$

$$SO_4^{\circ-} + SO_4^{\circ-} \rightarrow S_2O_8^{2-} \quad (10)$$

$$HO^{\circ} + SO_4^{\circ-} \rightarrow HSO_5^- \quad (11)$$

$$HO\cdot + HO\cdot \rightarrow H_2O_2 \quad (12)$$

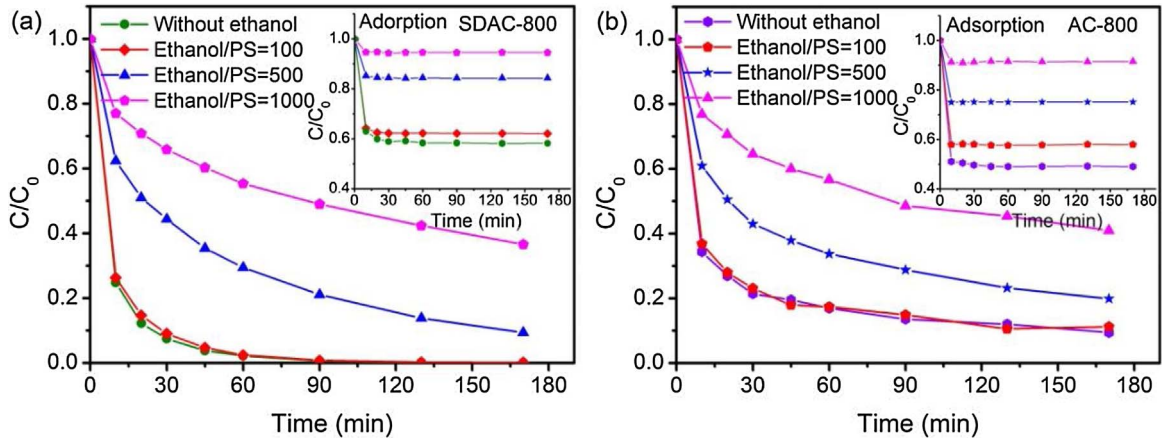

Fig. 8. Effect of ethanol on 4CP degradation with (a) SDAC-800/PS, and (b) AC-800/PS. Reaction conditions: $[4CP]_0$ = 80 mg L^{-1}, catalyst = 0.1 g L^{-1}, [PS] = 15 mM, and temperature = 25 °C.

$$SO_4^{\cdot -} + S_2O_8^{2-} \rightarrow SO_4^{2-} + S_2O_8^{\cdot -} \quad (13)$$

4. Conclusion

In summary, sulfur-doped hierarchically porous carbons with both structural and compositional modification were successfully synthesized by using low cost of thiophene as sulfur/carbon precursor and KOH as activator. Experiment results demonstrated that the catalytic oxidation performance of these resulting samples were significantly influenced by their annealing temperature, where the sample treated at 800 °C (SDAC-800) showed the best catalytic activity for 4CP degradation with PS. Characterizations suggested that the increasing concentration of sp2 carbon structure, electron-rich C=O groups, defective sites, and the significant removal of acidic sulphone groups at elevated annealing temperature contributed to the high catalytic activity of SDAC-800. The superior performance of SDAC-800 in PS activation to AC-800 and rGO demonstrated that sulfur doping played an important role in catalytic activity enhancement. Associated with quenching tests, it is suggested that the conventional radical pathway was not a critical role in 4CP degradation. In contrast, the process was controlled by both particle-surface interaction and non-radical pathway, and the latter played a dominant role. The excellent catalytic activity and good general applicability of the SDAC-800 make it to be a very promising metal-free catalyst for wastewater treatment. This study not only gives further insight into the mechanism of PS activation with S-doped activated carbon, but also provides a green, low-cost, and efficient approach for synthesis highly reactive catalyst for environmental remediation.

Acknowledgments

The authors gratefully acknowledge the financial support from the Shanxi Province Science Foundation for Youths (2014021016-3), the National Natural Science Foundation of China (21507140), and the Strategic Priority Research Program of the Chinese Academy of Sciences (XDA07030300).

Appendix A. Supplementary data

Supplementary data associated with this article can be found, in the online version, at http://dx.doi.org/10.1016/j.apcatb.2017.08.073.

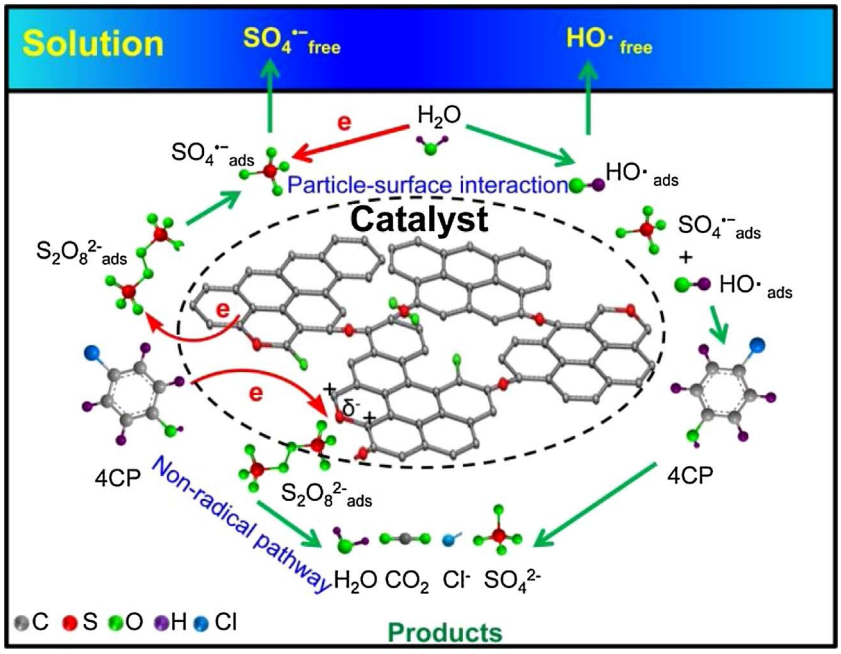

Scheme 1. Mechanism of PS activation on sulfur-doped hierarchically porous carbon.

References

[1] S. Indrawirawan, H. Sun, X. Duan, S. Wang, J. Mater. Chem. A 3 (2015) 3432–3440.
[2] H. Sun, X. Yang, L. Zhao, T. Xu, J. Lian, J. Mater. Chem. A 4 (2016) 9455–9465.
[3] P. Shukla, H. Sun, S. Wang, H.M. Ang, M.O. Tadé, Sep. Purif. Technol. 77 (2011) 230–236.
[4] M. Pera-Titus, V. García-Molina, M.A. Baños, J. Giménez, S. Esplugas, Appl. Catal. B 47 (2004) 219–256.
[5] W.-D. Oh, Z. Dong, T.-T. Lim, Appl. Catal. B 194 (2016) 169–201.
[6] X. Duan, Z. Ao, H. Sun, S. Indrawirawan, Y. Wang, J. Kang, F. Liang, Z.H. Zhu, S. Wang, ACS Appl. Mater. Interfaces 7 (2015) 4169–4178.
[7] P. Wang, S. Yang, L. Shan, R. Niu, X. Shao, J. Environ. Sci. 23 (2011) 1799–1807.
[8] S. Yang, X. Yang, X. Shao, R. Niu, L. Wang, J. Hazard. Mater. 186 (2011) 659–666.
[9] G.P. Anipsitakis, D.D. Dionysiou, Appl. Catal. B 54 (2004) 155–163.
[10] S. Yang, P. Wang, X. Yang, L. Shan, W. Zhang, X. Shao, R. Niu, J. Hazard. Mater. 179 (2010) 552–558.
[11] S.A. Kordkandi, M. Forouzesh, J. Taiwan Inst. Chem. E 45 (2014) 2597–2604.
[12] G.P. Anipsitakis, D.D. Dionysiou, Environ. Sci. Technol. 38 (2004) 3705–3712.
[13] G.P. Anipsitakis, D.D. Dionysiou, M.A. Gonzales, Environ. Sci. Technol. 40 (2006) 1000–1007.
[14] Q. Ji, J. Li, Z. Xiong, B. Lai, Chemosphere 172 (2017) 10–20.
[15] J. Li, Q. Liu, Q.Q. Ji, B. Lai, Appl. Catal. B 200 (2017) 633–646.
[16] X. Duan, C. Su, L. Zhou, H. Sun, A. Suvorova, T. Odedairo, Z. Zhu, Z. Shao, S. Wang, Appl. Catal. B 194 (2016) 7–15.
[17] H. Lee, H.I. Kim, S. Weon, W. Choi, Y.S. Hwang, J. Seo, C. Lee, J.H. Kim, Environ. Sci. Technol. 50 (2016) 10134–10142.
[18] P.R. Shukla, S. Wang, H. Sun, H.M. Ang, M. Tadé, Appl. Catal. B 100 (2010) 529–534.
[19] X.-R. Xu, X.-Z. Li, Sep. Purif. Technol. 72 (2010) 105–111.
[20] I. Hussain, Y. Zhang, S. Huang, X. Du, J. Chem. Eng. 203 (2012) 269–276.
[21] Y. Ren, L. Lin, J. Ma, J. Yang, J. Feng, Z. Fan, Appl. Catal. B 165 (2015) 572–578.
[22] S.B. Hammouda, F. Zhao, Z. Safaei, V. Srivastava, D. Lakshmi Ramasamy, S. Iftekhar, S. kalliola, M. Sillanpää, Appl. Catal. B 215 (2017) 60–73.
[23] R.R. Solís, F.J. Rivas, O. Gimeno, Appl. Catal. B 200 (2017) 83–92.
[24] E. Saputra, S. Muhammad, H. Sun, S. Wang, RSC Adv. 3 (2013) 21905.
[25] H. Sun, S. Liu, G. Zhou, H.M. Ang, M.O. Tade, S. Wang, ACS Appl. Mater. Interface 4 (2012) 5466–5471.
[26] X.-Y. Xu, G.-M. Zeng, Y.-R. Peng, Z. Zeng, Chem. Eng. J. 200–202 (2012) 25–31.
[27] W. Peng, S. Liu, H. Sun, Y. Yao, L. Zhi, S. Wang, J. Mater. Chem. A 1 (2013) 5854.
[28] H. Lee, H.-J. Lee, J. Jeong, J. Lee, N.-B. Park, C. Lee, J. Chem. Eng. 266 (2015) 28–33.
[29] H. Chen, K.C. Carroll, Environ. Pollut. 215 (2016) 96–102.
[30] W. Kiciński, A. Dziura, Carbon 75 (2014) 56–67.
[31] S. Liu, W. Peng, H. Sun, S. Wang, Nanoscale 6 (2014) 766–771.
[32] H. Sun, C. Kwan, A. Suvorova, H.M. Ang, M.O. Tadé, S. Wang, Appl. Catal. B 154–155 (2014) 134–141.
[33] X. Duan, K. O'Donnell, H. Sun, Y. Wang, S. Wang, Small 11 (2015) 3036–3044.
[34] R.S. Ribeiro, A.M.T. Silva, J.L. Figueiredo, J.L. Faria, H.T. Gomes, Carbon 62 (2013) 97–108.
[35] X. Wang, Y. Qin, L. Zhu, H. Tang, Environ. Sci. Technol. 49 (2015) 6855–6864.
[36] W. Tian, H. Zhang, X. Duan, H. Sun, M.O. Tade, H.M. Ang, S. Wang, ACS Appl. Mater. Interface 8 (2016) 7184–7193.
[37] W. Kiciński, M. Szala, M. Bystrzejewski, Carbon 68 (2014) 1–32.
[38] Y. Guo, Z. Zeng, Y. Li, Z. Huang, J. Yang, Sep. Purif. Technol. 179 (2017) 257–264.
[39] S. Morales-Torres, A.M.T. Silva, F.J. Maldonado-Hódar, B.F. Machado, A.F. Pérez-Cadenas, J.L. Faria, J.L. Figueiredo, F. Carrasco-Marín, Appl. Catal. B 105 (2011) 86–94.
[40] C. Liang, C.F. Huang, N. Mohanty, R.M. Kurakalva, Chemosphere 73 (2008) 1540–1543.
[41] M. Seredych, T.J. Bandosz, Carbon 49 (2011) 1216–1224.
[42] H.L. Poh, P. Simek, Z. Sofer, M. Pumera, ACS Nano 7 (2013) 5262–5272.
[43] Z. Yang, Z. Yao, G. Li, G. Fang, H. Nie, Z. Liu, X. Zhou, X. Chen, S. Huang, ACS Nano 6 (2012) 205–211.
[44] J.E. Park, Y.J. Jang, Y.J. Kim, M.S. Song, S. Yoon, D.H. Kim, S.J. Kim, Phys. Chem. Chem. Phys. 16 (2014) 103–109.
[45] A.P. Terzyk, Colloids Surf. A Physicochem. Eng. Asp. 177 (2001) 23–45.
[46] C.H. Choi, S.H. Park, S.I. Woo, Green Chem. 13 (2011) 406–412.
[47] M. Tammer, G. Sokrates, Infrared and Raman Characteristic Group Frequencies: Tables and Charts, Wiley, Chichester, 2004.
[48] T. Enoki, S. Fujii, K. Takai, Carbon 50 (2012) 3141–3145.
[49] B. Frank, J. Zhang, R. Blume, R. Schlogl, D.S. Su, Angew. Chem. Int. Ed. 48 (2009) 6913–6917.
[50] Y. Wang, Z. Ao, H. Sun, X. Duan, S. Wang, Appl. Catal. B 198 (2016) 295–302.
[51] Y. Deng, C.M. Ezyske, Water Res. 45 (2011) 6189–6194.
[52] B.-T. Zhang, Y. Zhang, Y. Teng, M. Fan, Crit. Rev. Environ. Sci. Technol. 45 (2014) 1756–1800.
[53] X. Duan, H. Sun, Y. Wang, J. Kang, S. Wang, ACS Catal. 5 (2015) 553–559.
[54] X. Duan, Z. Ao, L. Zhou, H. Sun, G. Wang, S. Wang, Appl. Catal. B 188 (2016) 98–105.